Acta Cryst. (1968). A **24**, 117

High-Resolution Monochromatization of Neutrons and X-rays by Multiple Bragg Reflection*

BY D. A. KOTTWITZ
Battelle Memorial Institute, Pacific Northwest Laboratory, Richland, Washington, U.S.A.

(*Received* 17 *January* 1967)

A simple scheme for obtaining highly monochromatic, reproducible beams of slow neutrons or X-rays at fixed wavelengths by means of crystal diffraction is described. The method is based on the well-known phenomenon of 'umweganregung', in which a 'forbidden' Bragg reflection is simulated under conditions of multiple reflection, *i.e.* when three or more reciprocal lattice points lie on an Ewald sphere. It is shown that there are orientations at which the Bragg angle (and wavelength) of a simulated reflection has local maxima. With only coarse collimation in the neighborhood of these extrema, perfect crystals can give wavelength resolutions of $\Delta\lambda/\lambda \simeq 10^{-5}$. Mosaic crystals would give less resolution but greater intensity. Since the various simulations of a 'forbidden' reflection may interfere with each other, it is necessary to carry out systematic computer calculations to check for interference after the extrema have been located. The scheme is applicable to a large set of crystals, including several diamond-structure and hexagonal close-packed elements and compounds such as quartz and calcite. Detailed numerical results show that germanium can reflect about 80 potentially useful wavelengths in the range 1·2 to 5 Å (neutron energy 0·003 to 0·05 eV). A number of other interesting properties of such beams are pointed out. Potential uses in neutron research and several problems are discussed briefly.

1. Introduction

In recent years the flux of thermal neutrons in some advanced research reactors has approached 10^{15}n.cm^{-2}.sec^{-1} (Hendrie, 1965; Swartout, Boch, Cole, Cheverton, Adamson & Winters, 1965). Such increased source intensity makes it possible to consider substantial improvements in energy resolution for many experiments using slow-neutron beams. The purpose of this paper is to describe a relatively simple method of obtaining highly monochromatic beams of slow neutrons at fixed energies in the range 0·003 to 0·05 eV (wavelength range 1·2 to 5 Å). Although attention is directed mainly toward neutrons, the basic scheme and much of the discussion apply equally well to X-rays.

It has been known for several years that multiple Bragg reflection (sometimes 'simultaneous diffraction' or 'multiple diffraction') in crystal spectrometers can produce complicated disturbing effects on measurements of slow-neutron spectra (Hay, 1959; Spencer & Smith, 1960). These disturbances, which arise when a second set of lattice planes simultaneously satisfies the Bragg condition for the same wavelength, may take two rather distinct extreme forms. The occurrence of multiple reflection tends to reduce the intensity of a normally strong primary reflection; this effect accounts for dips often seen in measured spectra. On the other hand, multiple reflection may increase the intensity of a normally weak reflection. The latter effect is seen most dramatically when a 'forbidden' reflection is simulated under conditions of multiple reflection. This is the celebrated case of 'umweganregung' (Renninger, 1937), which is now a well understood phenomenon in the diffraction of X-rays, electrons, and neutrons. It is possible to describe this effect qualitatively as follows. The reflected beam produced by the second set of Bragg planes is in turn reflected by a third set of planes, which automatically has the necessary orientation. Furthermore, this doubly reflected beam has exactly the same direction as a beam reflected directly from the primary set of Bragg planes. Of course, both the second and third sets of planes must have non-zero structure factors. The third set of planes is uniquely determined by the condition

$$\mathbf{K}_1 = \mathbf{K}_2 + \mathbf{K}_3, \qquad (1)$$

where $\mathbf{K}_n$ is the reciprocal lattice vector corresponding to the nth set of planes. In this paper the second and third sets of planes, which cooperate to simulate a 'forbidden' primary reflection, are called the secondary and tertiary planes. A detailed discussion of these points and many references to the extensive literature of multiple Bragg reflection may be found in the recent review article of Terminasov & Tuzov (1964).

In the following sections it will be shown that under certain conditions, a 'forbidden' reflection simulated by multiple Bragg reflection may have a high degree of monochromaticity. Detailed results will be presented for germanium as an example. In addition, other interesting properties of the resulting beam, various problems, and possible uses will be discussed.

2. Algebraic conditions for multiple Bragg reflection

The mathematical conditions for multiple Bragg reflection have been presented in various forms in recent papers (Hay, 1959; Spencer & Smith, 1960; Cole, Chambers & Dunn, 1962). The equations which are most convenient for our present purposes are slightly different; thus a brief derivation and discussion are necessary.

* Work performed under U.S.A.E.C. Contract AT(45-1)-1830.

Let us assume a conventional spectrometer in which both the incident and primary diffracted beams are horizontal. Thus the primary Bragg planes are vertical, and the orientation of the crystal may be completely specified by the Bragg angle θ and the azimuthal angle α between the vertical unit vector $\mathbf{V}$ and an arbitrary vector $\mathbf{Z}$ lying fixed in the primary Bragg plane, as in Fig. 1. Also shown are the reciprocal lattice vector $\mathbf{K}_1$ corresponding to the primary Bragg planes, and the wave vector $\mathbf{k}$ of the incident beam ($k=1/\lambda$).

The Laue–Bragg condition for reflection from the primary Bragg planes is

$$\mathbf{k}\cdot\mathbf{K}_1=-\tfrac{1}{2}K_1^2. \tag{2}$$

Similarly, for simultaneous reflection from the secondary Bragg planes corresponding to the reciprocal lattice vector $\mathbf{K}_2$,

$$\mathbf{k}\cdot\mathbf{K}_2=-\tfrac{1}{2}K_2^2. \tag{3}$$

After substituting

$$\mathbf{k}=k(\mathbf{K}_1\times\mathbf{V}\cos\theta-\mathbf{K}_1\sin\theta)/K_1,$$

and eliminating k, we get

$$\tan\theta=[\mathbf{V}\cdot(\mathbf{K}_2\times\mathbf{K}_1)]/[\mathbf{K}_2\cdot(\mathbf{K}_1-\mathbf{K}_2)]. \tag{4}$$

From the relation

$$\mathbf{V}=[\mathbf{Z}\cos\alpha+(\mathbf{Z}\times\mathbf{K}_1/K_1)\sin\alpha]/Z$$

it readily follows that

$$\tan\theta=[\mathbf{Z}\cdot(\mathbf{K}_2\times\mathbf{K}_1)\cos\alpha+K_1(\mathbf{Z}\cdot\mathbf{K}_2)\sin\alpha]/Z\mathbf{K}_2\cdot\mathbf{K}_3, \tag{5}$$

where $\mathbf{K}_3$ is defined in equation (1). This result shows that $\tan\theta$ depends sinusoidally on the azimuthal angle α (with a change of phase). It may then be written finally in the simple form

$$\tan\theta=\tan\theta_p\cos(\alpha-\alpha_p), \tag{6}$$

where

$$\tan\theta_p\equiv R/|S| \tag{7a}$$

$$\cos\alpha_p\equiv\mathbf{Z}\cdot\mathbf{R}|S|/ZRS \tag{7b}$$

$$\sin\alpha_p\equiv K_1(\mathbf{Z}\cdot\mathbf{K}_2)|S|/ZRS \tag{7c}$$

$$\mathbf{R}\equiv\mathbf{K}_2\times\mathbf{K}_1=\mathbf{K}_2\times\mathbf{K}_3=\mathbf{K}_1\times\mathbf{K}_3 \tag{7d}$$

$$S\equiv\mathbf{K}_2\cdot\mathbf{K}_3. \tag{7e}$$

The two parameters θ_p and α_p have direct geometrical significance. Equation (7*a*) shows that θ_p, the maximum value of the Bragg angle, is the acute angle between the secondary and tertiary Bragg planes, while equation (7*b*) shows that α_p, the corresponding value of the azimuthal angle, is the angle (with due regard for signs) between the reference vector $\mathbf{Z}$ and the zone axis $\mathbf{R}$ of the three reflections.

In Fig. 2 are plotted three examples of equation (6), each curve corresponding to a different secondary reflection vector $\mathbf{K}_2$. Curves similar to these have been discussed by several investigators (Hay, 1959; Spencer & Smith, 1960; Cole, Chambers & Dunn, 1962). We shall refer to them as 'multiple-reflection curves'.

The basis for the proposed scheme of monochromatization may be established directly from Fig. 2.

Let us suppose that the case is one of 'umweganregung', in which a 'forbidden' primary reflection corresponding to $\mathbf{K}_1$ may be simulated by the cooperative action of two reflections corresponding to $\mathbf{K}_2$ and $\mathbf{K}_3$. Then each multiple-reflection curve in Fig. 2 indicates the orientations (and, *via* Bragg's law, the wavelengths) for which simulation by a cooperating pair of planes may occur. Each curve has a simple shape with a single maximum value of $\theta=\theta_p$ at $\alpha=\alpha_p$. This extremum is the basis for high-resolution monochromatization, since the Bragg angle θ and the wavelength λ are stationary (to second order) for variations of the orientation angle α. Thus if the crystal has an orientation corresponding to α_p and θ_p, only a very narrow range of wavelengths is transmitted, even when the collimators have finite angular divergence.

Let us then designate an extremum corresponding to α_p and θ_p as an 'operating point'. In Fig. 2, two operating points are enclosed in rectangular windows intended to represent arbitrary degrees of collimation. Inspection of Fig. 2 shows that another multiple-reflection curve may pass so close to an operating point that it crosses the window and contributes an inseparable reflection of ordinary resolution. This constitutes a type of 'interference' which renders an operating point useless for high-resolution monochromatization. Thus the neighborhood of each operating point must be checked for interference by the other curves.

An additional complication now arises from the fact that the Bragg angle θ has the nature of an angle of latitude on a sphere, and α has the nature of an angle of longitude. Thus true angular relationships are distorted in a graph such as Fig. 2, particularly for large values of θ. In order to understand these points more fully, it is useful to proceed geometrically.

It should be pointed out here that singular cases of equation (6) sometimes occur, *i.e.* when $\theta_p=90$ or $0°$. The former case, which is illustrated in Fig. 2, never gives a useful operating point but may cause interfer-

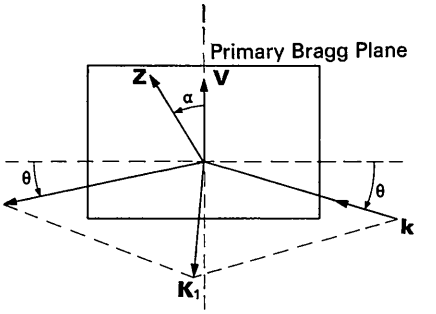

Fig. 1. Spectrometer geometry. The incident and diffracted beams are horizontal, and the reference vector $\mathbf{Z}$ lies fixed in the vertical primary Bragg plane. $\mathbf{V}$ is a vertical unit vector.

ence. The latter case is never of experimental interest, but may have to be dealt with in a computer program. Finally it must be pointed out that occasionally two or more curves have the same values of α_p and θ_p and thus coincide exactly. This situation, however, does not constitute interference in the present sense.

3. Geometry of multiple Bragg reflection

Consideration of the geometrical relationships of multiple Bragg reflection leads to a better understanding of interference between multiple-reflection curves, of singular cases, and of coincidence of curves. For greater clarity we adopt a different geometrical standpoint in this section. The crystal is considered to be *fixed* in space with both the primary and secondary Bragg planes vertical, while the direction of the incident beam is completely *variable* and no longer constrained to be horizontal. In Fig. 3, the origin O is located at an arbitrary point of the reciprocal lattice, and the points P_1 and P_2 are reciprocal lattice points corresponding to the horizontal reciprocal lattice vectors $\mathbf{K}_1$ and $\mathbf{K}_2$, respectively. Consider the planes which perpendicularly bisect the vectors $\mathbf{K}_1$ and $\mathbf{K}_2$; these are represented in Fig. 3 by the triangles CQS and CRS, respectively. The Laue-Bragg condition for the primary plane, equation (2), is satisfied by any wave vector $\mathbf{k}$ joining the plane CQS to the origin. Similarly, equation (3) is satisfied by any wave vector joining the plane CRS to the origin. Provided that $\mathbf{K}_1$ and $\mathbf{K}_2$ are not parallel, both equations are satisfied on the intersection of the planes, represented by the vertical line $\overline{SC}$. Thus any direction of incidence lying in the plane OCS gives multiple Bragg reflection for an appropriate wavelength.

Let $\overline{SO}$ represent an arbitrary incident wave vector $\mathbf{k}$ for which multiple reflection occurs. S is equidistant from the three reciprocal lattice points – O, P_1 and P_2 – and it is the center of an Ewald sphere. The shortest possible vector $\mathbf{k}$ is the one lying in the plane OP_1P_2; it is represented by $\overline{CO}$. The point C is the center of a circle which passes through the points – O, P_1 and P_2. Also indicated in Fig. 3 are various important angles. The general Bragg angle θ corresponding to $\mathbf{k}=\overline{SO}$ is shown, as well as the maximum Bragg angle θ_p which occurs when $\mathbf{k}=\overline{CO}$. The angle δ is the azimuthal angle measured with respect to the value α_p which corresponds to the maximum θ_p, *i.e.*

$$\delta \equiv \alpha - \alpha_p. \tag{8}$$

The angle β specifies the direction of the incident beam within the plane OCS of possible directions.

The singular case in which $\theta_p = 90°$ arises when the center C of the circle coincides with the bisecting point Q. There is still a plane of possible incident directions for multiple reflection; it corresponds to

$$\delta \equiv \alpha - \alpha_p = \pm 90° \tag{9}$$

for all values of θ, as shown in Fig. 2. The singular case in which $\theta_p = 0$ corresponds to a circle of infinite radius and does not arise for finite, nonparallel vectors $\mathbf{K}_1$ and $\mathbf{K}_2$.

Consideration of Fig. 3 shows that, if a fourth point P_3 of the reciprocal lattice lies on the circle OP_1P_2, then the multiple-reflection curve given by equation (6) for the secondary Bragg planes corresponding to P_3 coincides with the curve for P_2. This follows from the fact that the line $\overline{SC}$, the circle OP_1P_2, and the related angles are identical for the two cases. It is not surprising that coincident curves occur frequently during the simulation of reflection from a highly symmetrical primary plane, such as Ge {200}.

In order to study further the question of interference between multiple-reflection curves, it is useful to look at the geometry of Fig. 3 from a different point of view. Fig. 4 shows a coordinate sphere (not an Ewald sphere) centered on the origin O and viewed in a direction almost parallel to $\mathbf{k}$. Since only angles and directions have significance, the radius is arbitrarily chosen to be $\overline{OP_1}$ for clarity and convenience. As before $\overline{OP_1}$ is equal to $\mathbf{K}_1$, while $\overline{S'O}$ and $\overline{C'O}$ are segments of the infinite lines defined by $\overline{OS}$ and $\overline{OC}$. In addition the radii OB, $\overline{OA}$, and $\overline{OD}$ are parallel to QC, $\overline{QS}$, and $\overline{CS}$, respectively. P_1 is the pole, and the great circle BAD is the equator, of a set of spherical coordinates based on θ and δ (or θ and α). The great circle $C'S'D$ is the intersection of the sphere with the plane OCS and thus defines the locus of incident directions for which multiple reflection by $\mathbf{K}_1$ and $\mathbf{K}_2$ occurs. The operating point, which is given by $\theta=\theta_p$ and $\delta=0$, is represented by the point C'. As before, β is the angle between the incident direction corresponding to the operating point C' and an arbitrary incident direction in the plane $OC'S'$ of possible directions. Thus Fig. 4 shows that the natural variable to use for studying the neighborhood of C' for interference by other curves is β, instead of α. For a conventional spectrometer in which the reflecting Bragg

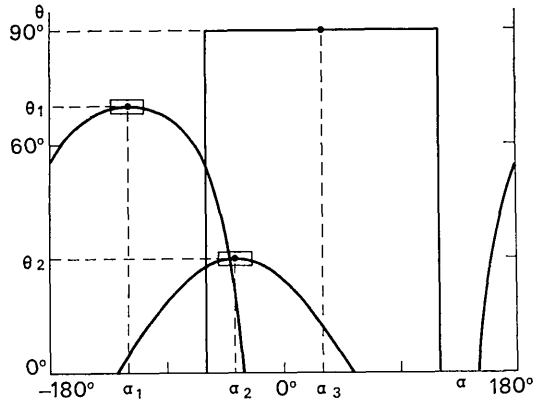

Fig. 2. Schematic plot of three multiple-reflection curves, Bragg angle θ *vs.* azimuthal angle α. Two extrema or operating points are enclosed in rectangular windows. The operating point at (α_2, θ_2) is subject to interference by one of the curves.

planes are vertical, β is the vertical deviation angle, limited by vertical collimation. One may now imagine an angular window of width $2\Delta\theta$ and height $2\Delta\beta$ (determined by collimation considerations) centered on the operating point C'. If any of the other multiple-reflection curves cross the window, then the operating point is useless for high-resolution monochromatization because of interference. A diamond-shaped window of this type is sketched in Fig. 4.

Reconsideration of Fig. 3 shows that every case of multiple Bragg reflection involving the primary reciprocal lattice point P_1 and any other reciprocal lattice point, such as P_4, leads to a 'fan' of possible incident directions lying in a plane passing through the origin, similar to plane OCS. The intersection of such a plane with the coordinate sphere in Fig. 4 is always a great circle. Segments XY and WZ of two such great circles are shown there; the former does not interfere with C', while the latter does. It is now clear that the distortion of angular relationships encountered in Fig. 2 may be avoided by a simple spherical map, in which the multiple-reflection curves are great circles.

Another observation that may be made from Fig. 4 is that the angles β and θ_p may be considered as the latitude and azimuth, respectively, in a spherical coordinate system based on the point D as pole and great circle $P_1C'B$ as equator. Note that this coordinate system depends on both $\mathbf{K}_1$ and $\mathbf{K}_2$, while the (α, θ)-coordinate system depends on $\mathbf{K}_1$ and $\mathbf{Z}$ only. Furthermore it should be pointed out that the reflected beam produced by simulated reflection (having wave vector $\mathbf{k}+\mathbf{K}_1$) also is restricted to a fan of directions lying in a plane.

Finally it is necessary to derive some equations involving β. From Fig. 3 and equation (8) it immediately follows that

$$\tan\beta=\tan\delta\cos\theta_p=\tan(\alpha-\alpha_p)\cos\theta_p. \quad (10)$$

Similarly from Fig. 3 comes a set of three equivalent relationships,

$$k_p=k\cos\beta \quad (11a)$$

$$\lambda=\lambda_p\cos\beta \quad (11b)$$

$$\sin\theta=\sin\theta_p\cos\beta, \quad (11c)$$

where k_p and λ_p are the values of k and λ at the operating point.

4. Conditions for high-resolution monochromatization

It is now possible to summarize the conditions under which useful high-resolution monochromatization may occur. First, it is necessary to have a 'forbidden' reflection which can be simulated by 'umweganregung' in multiple Bragg reflection. For each such simulation there is an 'operating point', *i.e.* an orientation for which the reflected wavelength is a second-order extremum. Thus even with relatively crude collimation, only a very small range of wavelengths is reflected, provided that the operating point is not too close to another multiple reflection. This means that after an operating point has been located by calculation, it is necessary to determine whether the other multiple-reflection curves interfere with it. The size of the window which must be checked depends on the degree of collimation contemplated.

It should be pointed out here that 'monochromatic' beams produced by the multiple-reflection method may contain wavelengths corresponding to higher or lower orders of the nominal wavelength. Of course, a useful monochromator crystal must satisfy the usual requirements of small absorption, incoherent scattering, and inelastic scattering.

5. 'Forbidden' reflections

As Renninger (1937) pointed out in his original paper on 'umweganregung', different types of 'forbidden' Bragg reflections must be considered separately, depending on whether they are forbidden by: (1) the space lattice, (2) the space group, or (3) special atomic positions (*International Tables for X-ray Crystallography*, 1952). Each of these types will be discussed in turn, both in general terms and by means of examples for the diamond structure.

The first type of forbidden reflection occurs only for nonprimitive space lattices, each of which has its cha-

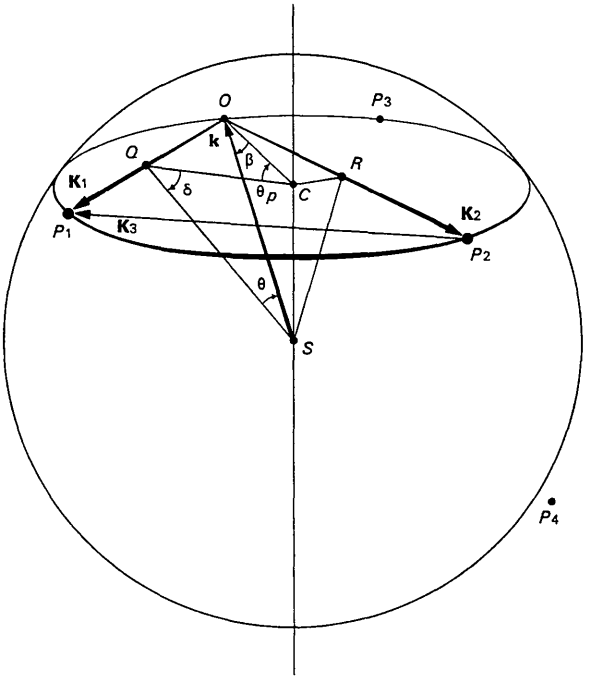

Fig. 3. Geometry of multiple Bragg reflection. $\mathbf{K}_1$, $\mathbf{K}_2$, and $\mathbf{K}_3$ are horizontal reciprocal-lattice vectors corresponding to the primary, secondary, and tertiary reflections, respectively. The center S of any Ewald sphere lies on the intersection SC of the planes CQS and CRS. The incident wave vector $\mathbf{k}$ is restricted to an 'fan' of directions lying in the vertical plane OCS.

racteristic set of absences or extinctions. For example, the face-centered cubic lattice of diamond rigorously forbids reflections having indices of mixed parity, such as 100 and 211. However, it is easily shown that forbidden reflections of this type cannot even be simulated by multiple Bragg reflection (Terminasov & Tuzov, 1964). Consequently, they may be completely ignored for our present purposes.

The second type of forbidden reflection occurs only for space groups containing a screw axis or glide plane; each such group has a characteristic set of absences. For example, the space group (*Fd3m*) of diamond forbids reflections *hk*0, where *h* and *k* are even and $h+k=4n+2$. Many (probably all) of these reflections, such as 200 and 420, which are rigorously forbidden by crystal symmetry, can be simulated by multiple reflection. Thus forbidden reflections of this type must be considered to be preeminent candidates for use in high-resolution monochromatization.

The third type of 'forbidden' reflection occurs for certain crystal structures with spherically symmetric scattering centers located at certain special positions in the unit cell. For example, the structure of diamond is such that spherically symmetric carbon atoms would give vanishing structure factors for reflections *hkl*, where *h*, *k*, and *l* are each even and nonzero, and $h+k+l=4n+2$. In general, however, crystal atoms are not expected to be spherically symmetric, and therefore such reflections are not strictly forbidden. In fact, weak but measurable 222 reflections of X-rays have been observed for diamond, germanium and silicon

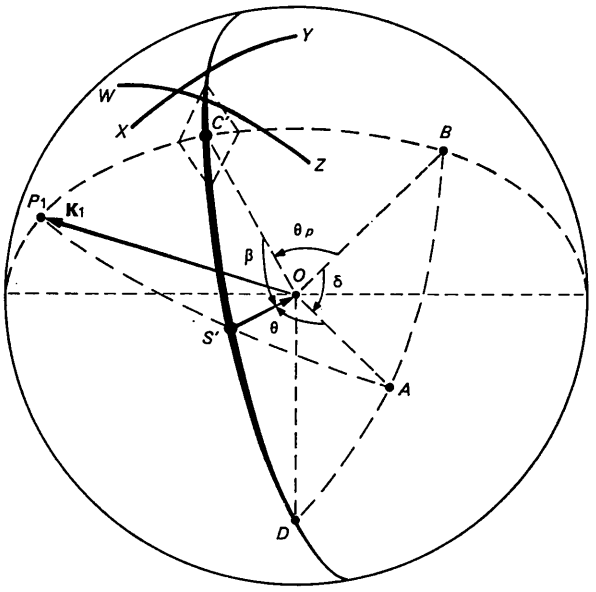

Fig. 4. Spherical mapping of multiple-reflection curves. The center of this coordinate sphere (not an Ewald sphere) is at the origin of the reciprocal lattice, and the viewing direction is almost parallel to the vector **k** of Fig. 3. The great circle *C'S'D* is a multiple-reflection curve, for which the operating point is *C'*. *XY* and *WZ* are segments of non-interfering and interfering curves, respectively.

(Renninger, 1960). Unfortunately even a weak 'forbidden' reflection could produce enough inseparable contamination to ruin the highly monochromatic component. Nevertheless, some of the 'forbidden' reflections of this type may still be useful for high-resolution monochromatization of neutrons, particularly in the case of cubic crystals, since at moderate temperatures in these crystals the nuclear 'cloud' which scatters neutrons does tend to be spherical. This suggests that it is worthwhile to investigate some of these reflections experimentally on an individual basis.

The foregoing discussion shows that many crystals are potentially suitable as high-resolution monochromators, since a substantial fraction of all crystals have glide planes or screw axes. These include many well-known compounds, such as calcite and α-quartz. However, there are two simple crystal structures which stand out from the rest because of the availability of large, high-quality crystals having desirable scattering and absorption properties. They are the diamond structure, exemplified by silicon and germanium, and the hexagonal close-packed structure, exemplified by beryllium, magnesium and zinc. All of these are probably useful for neutrons; many additional elements having the h.c.p. structure may also be suitable for X-rays (Lafourcade, Couderc & Larroque, 1965).

Like the diamond structure, the h.c.p. structure (space group $P6_3/mmc$) has 'forbidden' reflections of the second and third types. Reflections $hh2\bar{h}l$ having *l* odd are strictly forbidden (00$\bar{0}$1, 0003, 11$\bar{2}$1, *etc.*), while reflections *hkil* having *l* odd and $h-k=3n\neq 0$ are only approximately 'forbidden' (30$\bar{3}$1, 30$\bar{3}$3, 41$\bar{5}$1, *etc.*). Fortunately, several low-index reflections are of the former type, since the latter are less likely to be useful in hexagonal crystals, in which the nuclear 'clouds' have ellipsoidal shapes even at low temperatures.

6. Calculation for germanium

Because of the availability of large, almost perfect crystals of germanium and silicon and because of the simplicity of cubic symmetry, a computer program based on the equations and figures of §§2 and 3 has been written for the case of the diamond structure. The program, called DBSK3, is written in FORTRAN IV for the UNIVAC 1107 computer.

A brief description of the program scheme follows. For a given primary forbidden reflection $\mathbf{K}_1$ to be simulated and for a given reference vector **Z** lying in the primary Bragg planes, the program first finds all of the operating points inside any rectangle in the (α, θ) plane of Fig. 2, where the rectangle is defined by the lines: $\theta=\theta_{\min}$, $\theta=\theta_{\max}$, $\alpha=\alpha_{\min}$, and $\alpha=\alpha_{\max}$.

This is done by systematically computing equations (7) for all reciprocal lattice points inside a rectangular parallelepiped large enough to enclose all possible secondary reflections. After the operating points are ordered roughly in order of decreasing Bragg angle, each one is tested for interference by all other multiple-

reflection curves, including those which have their operating points outside the (α, θ) rectangle. To do this, a systematic test is made of all reciprocal lattice points inside a cube enclosing the Ewald sphere for the operating point. For reasons of computational simplicity, the (β, θ) region which is tested is not rectangular as indicated in Fig. 2, but is diamond-shaped as shown in Figs. 4 and 5. If interference is found to occur, that is, if a multiple-reflection curve crosses the diamond-shaped area as in Fig. 5, both β_i and $(\theta_i - \theta_p)$ are calculated. Often two or more curves produce interference. In any case, the four intersections (or corners of the diamond) which are nearest to the operating point define an asymmetric quadrilateral, shaded in Fig. 5, which may be characterized by the quantities θ_-, θ_+, β_-, and β_+. Thus the values of β_i and $(\theta_i - \theta_p)$ for each interfering curve provide a detailed picture of interference, while the four quantities θ_-, θ_+, β_-, and β_+ provide a summary by defining a region without interference. The program recognizes a coincident curve as a special case and does not treat it as an interfering curve.

A number of techniques have been used to decrease execution time for the program. For example, consideration of the structure factors of diamond-structure reflections shows that effective simulation can occur only for multiple reflections having all Miller indices odd; thus all systematic testing of reciprocal lattice points may be confined to these. Furthermore, for these odd indices the denominator in equation (7*a*) never vanishes; thus it is not necessary to provide for singular cases in which $\theta_p = 90°$. Fast preliminary tests are used to by-pass time-consuming detailed ones in the interference calculations, and integer arithmetic is frequently used. Finally, in operating the program it is often possible to save time by using symmetry considerations to reduce the range of the azimuthal angle α.

Calculations have been performed for the seven 'forbidden' reflections of germanium having the largest plane spacings: 200, 420, 244, 640, 222, 600, 622. In these calculations, the lattice constant of Ge was taken as 5·6576 Å, and the values of relevant physical constants as follows: Planck's constant $= 6{\cdot}6256 \times 10^{-27}$ erg sec, mass of neutron $= 1{\cdot}67482 \times 10^{-24}$ g, and charge of electron $= 1{\cdot}6021 \times 10^{-19}$ coulomb. Various parameters for the calculations are summarized in Table 1. In addition, the diamond-shaped region for testing interference has $\Delta\theta = 0{\cdot}5°$ and $\Delta\beta = 3°$ for all cases. The following arbitrary criteria were adopted in deciding whether an operating point is acceptable as a useful one: θ_- and $\theta_+ \geq 0{\cdot}25°$, and β_- and $\beta_+ \geq 1°$. As shown in the last column of Table 1, six of the seven forbidden reflections have more than 10 useful operating points. Detailed data on these operating points are given in Table 2. This table is self-explanatory, except that in columns 7 and 8 *X* indicates that θ_- or $\theta_+ \geqq 0{\cdot}5°$, and in columns 9 and 10 *Y* indicates that β_- or $\beta_+ \geq 3°$.

It is obvious that these results may be easily applied to diamond or silicon; the angles θ_p and α_p of the operating points are unchanged, while the wavelength λ_p and energy E_p are changed simply by constant factors which depend on the ratio of lattice constants. In summary, for germanium alone there are about 80 fixed wavelengths in the range 1·2 to 5 Å at which high-resolution monochromatization is possible, and both the number and range of values can be increased by using other crystals.

It is interesting to note that cases of coincident multiple-reflection curves occur frequently, especially for the 200 and 600 reflections. Thus any scheme developed to compute intensities and resolutions of simulated reflections ought to be broad enough to include them. Another significant point is that the range of Bragg angles is large, 15 to 85°, so that a spectrometer of special design might be needed to exploit the method fully.

7. Properties of the multiple-reflected beams

Now that the existence of a number of potentially useful operating points has been demonstrated, it is desirable to examine the properties of multiple-reflected beams in somewhat greater detail. The properties to be considered are monochromaticity, reproducibility, angular divergence, time-of-flight characteristics, intensity, and cross-sectional area.

The degree of monochromaticity depends on three independent factors: the intrinsic peak width of a perfect crystal, the mosaic width of an imperfect crystal, and the degree of collimation for the angle β. The analysis in §§ 2 and 3, which is based on the simple kinematic (or geometric) theory of diffraction, is adequate for determining a first approximation to the orientations and wavelengths for multiple Bragg reflection, but it erroneously gives an intrinsic peak width of zero. The more exact dynamical theory of diffraction, which has been reviewed recently by James (1963), is required to

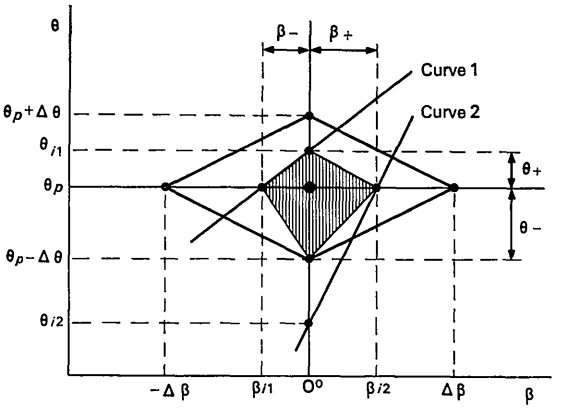

Fig. 5. Schematic details of interference calculations, Bragg angle θ *vs.* divergence angle β. Two interfering curves reduce the interference-free region from the diamond-shaped window to the shaded asymmetric quadrilateral which encloses the operating point.

Table 1. *Summary of parameters for calculations of simulated germanium reflections*

Column 7 gives the number of operating points (including coincident ones) found in the specified (α,θ)-rectangle. Column 8 gives the number of operating points (excluding coincidences) found to be free of interference.

Simulated reflection	Reference vector **Z**	θ_{min} (°)	θ_{max} (°)	α_{min} (°)	α_{max} (°)	Points tested	Points accepted
200	[001]	12	90	0	45	43	11
420	[001]	30	90	0	90	45	15
244	[01$\bar{1}$]	41	90	0	90	49	13
640	[001]	45	90	0	90	58	2
222	[01$\bar{1}$]	17	90	0	30	56	13
600	[001]	36	90	0	45	42	11
622	[01$\bar{1}$]	45	90	0	90	51	15

Table 2. *Operating points free of interference for 7 simulated germanium reflections*

In column 7 or 8, *X* indicates that θ_- or $\theta_+ \geq 0{\cdot}5°$, and in column 9 or 10, *Y* indicates that β_- or $\beta_+ \geq 3°$.

Primary (simulated) reflection	Secondary reflection	θ_p (°)	α_p (°)	λ (Å)	E (eV)	θ_- (°)	θ_+ (°)	β_+ (°)	β_+ (°)
200	11$\bar{1}$	70·52878	45·00000	5·33404	0·002875	*X*	*X*	*Y*	*Y*
	13$\bar{1}$	35·09680	18·43495	3·25289	0·007731	*X*	*X*	*Y*	*Y*
	31$\bar{1}$, $\bar{1}$1$\bar{1}$	29·49621	45·00000	2·78561	0·010542	*X*	*X*	*Y*	*Y*
	13$\bar{3}$	26·52535	45·00000	2·52665	0·012814	*X*	*X*	*Y*	*Y*
	33$\bar{1}$, $\bar{1}$3$\bar{1}$	25·94312	18·43495	2·47508	0·013353	*X*	*X*	*Y*	*Y*
	15$\bar{1}$	22·19161	11·30993	2·13690	0·017914	*X*	0·36	1·4	*Y*
	33$\bar{3}$, $\bar{1}$33	22·00171	45·00000	2·11953	0·018209	*X*	*X*	*Y*	*Y*
	15$\bar{3}$	19·46295	30·96375	1·88510	0·023019	*X*	*X*	2·7	*Y*
	37$\bar{1}$, $\bar{1}$7$\bar{1}$	14·94030	8·13010	1·45860	0·038449	0·47	0·40	*Y*	1·8
	35$\bar{5}$, $\bar{1}$5$\bar{5}$	14·94030	45·00000	1·45860	0·038449	*X*	*X*	*Y*	*Y*
	53$\bar{3}$, $\bar{3}$33	14·42007	45·00000	1·40891	0·041210	0·49	*X*	*Y*	*Y*
420	13$\bar{1}$	84·78409	24·09484	2·51968	0·012885	*X*	*X*	2·3	*Y*
	33$\bar{1}$	82·38862	36·69922	2·50786	0·013006	*X*	*X*	1·7	*Y*
	$\bar{1}$3$\bar{1}$	58·51784	17·71547	2·15772	0·017570	*X*	*X*	*Y*	*Y*
	$\bar{1}$1$\bar{1}$	56·25101	36·69922	2·10377	0·018483	*X*	*X*	*Y*	2·8
	35$\bar{1}$	48·50602	17·71547	1·89515	0·022776	*X*	*X*	1·0	1·3
	$\bar{1}$13	48·50602	65·90516	1·89515	0·022776	*X*	*X*	1·3	1·3
	$\bar{1}$5$\bar{1}$	46·91128	11·49046	1·84776	0·023959	*X*	*X*	2·5	2·1
	13$\bar{5}$	44·41531	65·90516	1·77074	0·026089	*X*	*X*	*Y*	1·8
	33$\bar{5}$	42·80175	74·97974	1·71915	0·027678	*X*	*X*	1·3	2·8
	35$\bar{3}$	42·71838	43·78057	1·71645	0·027765	0·49	*X*	1·4	1·7
	$\bar{1}$5$\bar{3}$	41·62296	31·37637	1·68059	0·028963	*X*	0·42	2·8	*Y*
	$\bar{3}$5$\bar{1}$	35·48970	9·75967	1·46890	0·037912	0·40	*X*	1·7	1·4
	37$\bar{1}$	34·22750	11·49046	1·42316	0·040388	0·41	0·25	1·5	1·1
	53$\bar{5}$	34·22750	84·88891	1·42316	0·040388	0·43	0·34	1·4	1·2
	$\bar{1}$37$\bar{7}$	31·03234	65·90516	1·30435	0·048081	0·33	*X*	1·1	1·1
244	1$\bar{1}$1	84·39959	56·30993	1·87686	0·023222	*X*	*X*	1·1	*Y*
	$\bar{1}$31	78·02327	36·86990	1·84482	0·024036	*X*	*X*	2·4	*Y*
	$\bar{1}$33	78·02327	0·00000	1·84482	0·024036	*X*	*X*	1·3	1·3
	3$\bar{1}$3	77·24659	50·19443	1·83934	0·024179	*X*	0·46	*Y*	1·9
	3$\bar{1}$1	75·23687	26·56505	1·82361	0·024598	*X*	*X*	1·1	2·9
	315	75·23687	63·43495	1·82361	0·024598	*X*	*X*	2·0	2·9
	3$\bar{1}$5	64·98282	66·03751	1·70894	0·028010	*X*	*X*	1·2	1·1
	335	63·88173	56·30993	1·69330	0·028530	*X*	*X*	*Y*	1·2
	3$\bar{3}$3	55·53404	56·30993	1·55483	0·033838	0·49	0·36	*Y*	1·5
	711	51·73730	0·00000	1·48074	0·037308	*X*	*X*	2·8	2·8
	5$\bar{1}\bar{1}$	51·21706	0·00000	1·47008	0·037851	*X*	*X*	2·3	2·3
	1$\bar{3}$1	48·14034	63·43495	1·40456	0·041465	*X*	*X*	2·5	2·2
	5$\bar{1}$7	43·78265	59·74356	1·30488	0·048042	*X*	*X*	1·6	1·4
640	313	82·38862	74·49864	1·55531	0·033816	*X*	*X*	2·1	2·1
	$\bar{1}$13	61·38895	65·19125	1·37753	0·043108	*X*	*X*	1·1	1·6
222	311	79·97501	0·00000	3·21654	0·007906	*X*	*X*	*Y*	*Y*
	3$\bar{1}$1	62·96431	30·00000	2·90947	0·009663	*X*	*X*	*Y*	*Y*
	3$\bar{1}\bar{1}$	51·49792	0·00000	2·55625	0·012519	*X*	*X*	*Y*	*Y*
	1$\bar{1}\bar{1}$	48·52706	0·00000	2·44742	0·013657	*X*	*X*	*Y*	*Y*
	5$\bar{1}$1	41·36036	19·10660	2·15842	0·017559	*X*	*X*	*Y*	1·4

Table 2 (*cont.*)

Primary (simulated) reflection	Secondary reflection	θ_p (°)	α_p (°)	λ (Å)	E (eV)	θ_- (°)	θ_+ (°)	β_- (°)	β_+ (°)
	511	41·03257	0·00000	2·14436	0·017790	*X*	*X*	*Y*	*Y*
	$5\bar{1}\bar{1}$	38·94244	0·00000	2·05307	0·019407	*X*	*X*	*Y*	*Y*
	$3\bar{3}\bar{1}$	35·47734	19·10660	1·89577	0·022761	*X*	*X*	1·8	1·8
	$5\bar{3}1$	34·04773	30·00000	1·82881	0·024458	*X*	*X*	2·8	2·8
	$5\bar{3}\bar{1}$	31·71867	13·89788	1·71732	0·027737	*X*	*X*	2·5	1·1
	711, $3\bar{3}\bar{3}$	27·21492	0·00000	1·49383	0·036657	*X*	*X*	2·6	2·6
	$7\bar{5}1$	23·07392	30·00000	1·28017	0·049915	*X*	0·46	1·9	1·9
	713	22·02350	19·10660	1·22486	0·054524	0·48	0·27	1·8	2·4
600	$33\bar{1}$	86·98304	18·43495	1·88325	0·023065	*X*	*X*	1·0	1·5
	$53\bar{1}$, $13\bar{1}$	75·23687	18·43495	1·82361	0·024598	*X*	*X*	2·9	2·9
	$1\bar{1}1$, $5\bar{1}1$, $33\bar{3}$	70·52878	45·00000	1·77801	0·025876	*X*	*X*	*Y*	*Y*
	$53\bar{3}$, $13\bar{3}$	62·94713	45·00000	1·67953	0·028999	*X*	*X*	2·0	2·0
	$55\bar{1}$, $15\bar{1}$	55·53404	11·30993	1·55483	0·033838	*X*	*X*	*Y*	1·5
	$35\bar{3}$	54·45125	30·96375	1·53438	0·034745	*X*	*X*	1·8	*Y*
	$73\bar{1}$, $\bar{1}3\bar{1}$	48·14034	18·43495	1·40456	0·041465	*X*	*X*	2·2	2·2
	$37\bar{1}$	45·97953	8·13010	1·35611	0·044481	*X*	*X*	2·9	2·3
	$71\bar{1}$, $\bar{1}1\bar{1}$, $55\bar{5}$, $15\bar{5}$	43·31385	45·00000	1·29369	0·048876	*X*	*X*	1·5	1·5
	$37\bar{3}$	43·00087	23·19859	1·28618	0·049449	*X*	0·39	1·4	1·8
	$57\bar{3}$, $17\bar{3}$	40·76669	23·19859	1·23143	0·053944	*X*	0·43	1·6	1·3
622	$5\bar{1}\bar{1}$	87·46950	0·00000	1·70417	0·028167	*X*	*X*	2·2	2·2
	$1\bar{1}\bar{1}$	84·94884	0·00000	1·69921	0·028332	*X*	*X*	1·5	1·5
	$33\bar{1}$	80·91528	90·00000	1·68443	0·028831	*X*	*X*	2·5	2·5
	$3\bar{3}1$	78·82001	47·86958	1·67346	0·029210	*X*	*X*	*Y*	1·1
	$5\bar{3}1$	72·97613	39·66403	1·63109	0·030747	*X*	*X*	2·5	*Y*
	$3\bar{3}\bar{1}$	71·64702	20·22954	1·61906	0·031206	*X*	0·37	1·0	1·2
	$5\bar{3}\bar{1}$	68·19625	16·77865	1·58380	0·032611	*X*	*X*	1·0	2·4
	711	66·15736	0·00000	1·56025	0·033603	*X*	*X*	1·4	1·4
	331	61·03992	47·86958	1·49253	0·036721	*X*	*X*	*Y*	1·1
	$3\bar{3}5$	60·76636	90·00000	1·48857	0·036917	*X*	*X*	2·2	2·2
	$7\bar{1}3$	59·31654	58·90907	1·46701	0·038010	*X*	*X*	1·2	1·3
	$3\bar{3}\bar{3}$	58·25416	0·00000	1·45062	0·038874	*X*	*X*	*Y*	*Y*
	$5\bar{3}\bar{3}$	57·73392	0·00000	1·44241	0·039317	*X*	*X*	2·5	2·5
	$35\bar{1}$	53·21158	28·93254	1·36612	0·043831	0·25	*X*	1·2	1·4
	$1\bar{5}3$	49·90221	73·22134	1·30487	0·048043	*X*	*X*	1·0	1·6

describe diffraction in crystals of finite size. One of the results of this fundamental theory is that the wavelengths and orientations which can give multiple diffraction are modified slightly, just as in the case of ordinary single diffraction (James, 1963; Bacon, 1962). In terms of Fig. 3 the locus of multiple Bragg reflection represented by the line $\overline{CS}$ is shifted and broadened by amounts of the order of $\Delta k/k \simeq 10^{-5}$. Thus for a perfect crystal the intrinsic wavelength resolution is

$$\Delta\lambda/\lambda \simeq \Delta k/k \simeq 10^{-5}. \qquad (12)$$

For a mosaic crystal, the peak width is determined by just those factors which operate in a double spectrometer (Compton & Allison, 1935), namely, the mosaic width, relative orientation, and interplanar spacings of the pair of cooperating Bragg planes which simulate the 'forbidden' reflection. Depending mainly on the mosaic, $\Delta\lambda/\lambda$ might range from 10^{-4} to 10^{-2}. Multiple Bragg reflection of neutrons in mosaic crystals has been studied recently by Moon & Shull (1964). The final factor which affects the monochromaticity for perfect and mosaic crystals is the vertical collimation angle $\Delta\beta$. From equation (11*b*) it immediately follows that

$$\Delta\lambda/\lambda = 1 - \cos\Delta\beta \cong (\Delta\beta)^2/2. \qquad (13)$$

Thus for $\Delta\beta \simeq \frac{1}{4}°$, $\Delta\lambda/\lambda \simeq 10^{-5}$. Equation (13) shows that the fractional resolution of a collimator is a constant independent of the Bragg angle.

The reproducibility of this well-defined wavelength is equally good since an operating point is determined by the constant angular relationships and lattice spacings inside the crystal and is located at an extremum with respect to external orientation. Thus only modest control of the crystal temperature and orientation is required to attain extremely good reproducibility.

For a perfect crystal the intrinsic divergence $\Delta\theta$ in the horizontal plane is given by

$$\Delta\theta \simeq \Delta k/k \simeq 10^{-5} \text{ radian} \simeq 2'' \qquad (14)$$

and is independent of any practical external collimation. The vertical divergence $\Delta\beta$ is determined by collimation, according to experimental needs for resolution and intensity. Thus the beam may be described as semiparallel.

An interesting time-of-flight characteristic may be noted from equation (11*a*), which shows that the horizontal component of momentum is constant (kinematic theory). Thus for neutrons, the horizontal component of velocity and the time-of-flight between vertical planes is independent of the degree of collimation. Unlike the wavelength and energy, which are merely stationary at the operating point, the time of flight is constant. Of course, this remark does not apply to X-rays.

Only rough estimates of beam intensities are possible without experiments or calculations employing the dynamical theory. However, it is reasonable to assume that crystal orientations and shapes will be found which give a reflection efficiency of about 50% for narrow wavelength and orientation bands given by equations (12) and (14). In that case the intensity is about 10^5 times smaller than for an ordinary single reflection from a mosaic crystal having $\Delta\lambda/\lambda = 10^{-2}$. Of course, if a mosaic crystal with $\Delta\lambda/\lambda = 10^{-3}$ were used for multiple-reflection monochromatization, the intensity would be about 10^3 times higher than for a perfect crystal. As usual, intensity and resolution requirements must be balanced against each other.

Since the multiple-reflection process is essentially self-collimating, it is not necessary to use pinholes or narrow slits to obtain a high degree of monochromaticity. Thus the cross-sectional area of a beam is limited primarily by the size of the monochromator, and areas of 10 cm^2 are feasible.

8. Various problems

There are a number of experimental and theoretical problems which remain to be dealt with in the study and use of high-resolution monochromatization. A major experimental problem is the removal of undesired components from the reflected beam. First, there are the various orders, both higher and lower, which are often present, as pointed out in § 4. They are likely to be extremely intense, but fortunately their wavelengths are usually quite different from the desired wavelength. Thus they can be removed or reduced by a variety of methods: control of the source spectrum, velocity selectors, horizontal collimation, and filters based on absorption, diffraction, or scattering. In addition, there is a general background of inelastic and incoherent scattered radiation of all wavelengths, which may be controlled by the same methods and also by the choice of the monochromator crystal itself. Another experimental problem in work of the highest precision would be radiation damage produced by fast neutrons in the monochromator.

In connection with the 'forbidden' reflections themselves, there are experimental and theoretical questions. As discussed in § 5, it is probable that some of the reflections in cubic crystals which are 'forbidden' only by special positions may still be useful for high-resolution monochromatization of neutrons. These must be investigated individually. In addition, however, there may even be difficulty with some reflections strictly forbidden by symmetry. For example, puzzling appearances of the 0001 reflection in three beryllium crystals have been reported for neutrons (Hay, Pattenden & Egelstaff, 1958). Thus it is necessary to confirm that the structure factors of potentially useful 'forbidden' reflections are in fact negligibly small.

Experimental measurements and calculations based on the dynamical theory of diffraction (James, 1963) are required to find the crystal orientations and shapes which are optimum for intensity and resolution, and to determine the deviations from the approximate kinematic theory. In passing, it should be noted that, in treating a diamond-structure crystal by means of dynamical theory, the multiple reflections having even indices must be considered explicitly; it is only in the kinematic theory that they may be ignored.

9. Potential uses

Since high resolution is obtained at high cost in intensity, many experiments, particularly those involving inelastic processes, are not feasible in the immediate future by means of the monochromatization method proposed here. However, experiments involving elastic scattering, particularly crystal diffraction and total reflection, are probably feasible at the present time. Some of these are mentioned below.

An obvious benefit of improved angular and wavelength resolution is increased precision in the determination of lattice and structure parameters, both chemical and magnetic. High-resolution beams of large cross-sectional area would also be useful in studying large scale imperfections in single crystals, *e.g.* lineage structures. Certainly the high degree of monochromaticity and reproducibility at fixed wavelengths can lead to highly precise standards of wavelength and energy for slow neutrons. The wavelengths at multiple-reflection operating points could thus become analogous to those of the characteristic X-rays. Finally, the unique energy, wavelength, and geometric properties of such beams might permit more precise determinations of parameters of the neutron itself, *e.g.* coherent scattering lengths.

The author wishes to acknowledge indebtedness to R. B. Smith for stimulating discussions and help in preliminary calculations.

References

Bacon, G. E. (1962). *Neutron Diffraction*, 2nd ed., p.55. Oxford: Clarendon Press.

Cole, H., Chambers, F. W. & Dunn, H. M. (1962). *Acta Cryst.* **15**, 138.

Compton, A. H. & Allison, S. K. (1935). *X-rays in Theory and Experiment*, 2nd ed., p.709. New York: Van Nostrand.

Hay, H. J. (1959) Report R-2982. Atomic Energy Research Establishment, Harwell, Berkshire, England.

HAY, H. J., PATTENDEN, N. J. & EGELSTAFF, P. A. (1958). *Acta Cryst.* **11**, 228.
HENDRIE, J. M. (1965). *Proc. 3rd Intern. Conf. Peaceful Uses of Atomic Energy*, **7**, 372. New York: United Nations.
International Tables for X-ray Crystallography (1952). Vol. I. Birmingham: Kynoch Press.
JAMES, R. W. (1963). *Solid State Physics*, **15**, 53.
LAFOURCADE, L., COUDERC, J.-J. & LARROQUE, P. (1965). *C.r. Acad. Sci. Paris*, **260**, 5752.
MOON, R. M. & SHULL, C. G. (1964). *Acta Cryst.* **17**, 805.
RENNINGER, M. (1937). *Z. Phys.* **106**, 141.
RENNINGER, M. (1960). *Z. Kristallogr.* **113**, 99.
SPENCER, R. R. & SMITH, J. R. (1960). *Nuclear Sci. & Eng.* **8**, 393.
SWARTOUT, J. A., BOCH, A. L., COLE, T. E., CHEVERTON, R. D., ADAMSON, G. M. & WINTERS, C. E. (1965). *Proc. 3rd Intern. Conf. Peaceful Uses of Atomic Energy*, **7**, 360. New York: United Nations.
TERMINASOV, YU. S. & TUZOV, L. V. (1964). *Usp. Phys. Nauk*, **83**, 223. For an English translation, see *Soviet Phys. Usp.* **7**, 434 (1964).

Acta Cryst. (1968). A**24**, 126

Étude Théorique de la Propagation des Rayons X dans un Cristal Parfait ou Legèrement Déformé

PAR A. AUTHIER,
Laboratoire de Minéralogie-Cristallographie, Sorbonne, Paris 5e, France
C. MALGRANGE
Laboratoire de Physique Théorique, Collège de France, Paris 5e, France
ET M. TOURNARIE
Centre d'Études Nucléaires de Saclay, France

(*Reçu le* 16 *juin* 1967)

Takagi's theory is used to calculate the propagation of X-rays in perfect and nearly perfect crystals. In the general case, the equations have to be solved on a computer. The principle of the calculation is given. It has been applied to the case where an incident plane wave is collimated by a slit. The separation of wave-fields is observed, each presenting a fine structure shown to be due to the diffraction by the slit. The same calculation is extended to a crystal submitted to a thermal gradient.The propagation and the intensities of wave-fields are in good agreement with the predictions of Penning and Polder.

Introduction

Nous nous sommes proposé d'étudier la propagation des rayons X dans un cristal déformé. Plusieurs théories ont été déjà développées dans ce but, en particulier celles de Penning & Polder (1961) et de Kato (1963*a*,*b*, 1964). Ces théories permettent de calculer le trajet des rayons dans un cristal légèrement déformé. Celle de Penning & Polder est plus commode pour calculer les trajets, celle de Kato repose sur des bases mathématiques plus précises et permet le calcul des phases. Elle se prête aisément à l'étude des franges de solution pendulaire dans les cristaux déformés (Kato & Ando, 1966; Hart, 1966). Ces théories, très agréables car elles n'exigent pas l'utilisation d'ordinateur puissant, ont certaines limitations. Par suite de leurs hypothèses de départ, elles ne sont plus valables lorsque la déformation est très grande, par exemple au voisinage d'une ligne de dislocation. D'autre part, si l'on veut suivre effectivement le trajet d'un rayon, il faut l'isoler par une fente. Par suite de la nature ondulatoire des rayonnements, on ne peut isoler un rayon mais un pinceau qui, par suite des phénomènes de diffraction, acquerra une structure fine. Les théories mentionnées plus haut ne sont pas armées pour cela.

Or, pour étudier expérimentalement le trajet de l'énergie et l'intensité de chaque champ d'ondes pour un écart à l'incidence de Bragg donné, il faut utiliser la double réfraction des rayons X: une onde plane incidente sur un cristal excite à l'intérieur deux champs d'ondes pour une direction de polarisation donnée. Cet effet a été prévu par Borrmann (1955) et mis en évidence par Authier (1960, 1961). Pour pouvoir observer la séparation des trajets des champs d'ondes, on place une fente dont la largeur optimale est de l'ordre de 50 μm sur le trajet d'une onde plane. Les pinceaux constitués par ces deux champs d'ondes ont une structure fine due à la diffraction par les bords de la fente. Elle a été observée et interprétée par Authier & Malgrange (1965). Nous l'avons analysée ici en détail.

Lorsque l'onde incidente sur un cristal est une onde quelconque, par exemple une onde sphérique, ou une onde plane limitée par une fente, la théorie fondamentale de Laue n'est plus directement applicable, pas plus que les théories citées plus haut. Une généralisation de la théorie dynamique au cas d'une onde sphérique a été donnée par Kato (1961*a*,*b*). Une autre théorie, applicable à toute forme d'onde incidente et au cas d'un cristal déformé a été donnée par Takagi (1962). C'est cette théorie que nous avons utilisée pour étudier